Effect of negative T-stress on R-curves for Si_3N_4-ceramics

Open Access at KIT

P. Zielonka, P. Hettich, S. Fünfschilling, G. Schell,
G. Rizzi, T. Fett

KIT SCIENTIFIC WORKING PAPERS 76

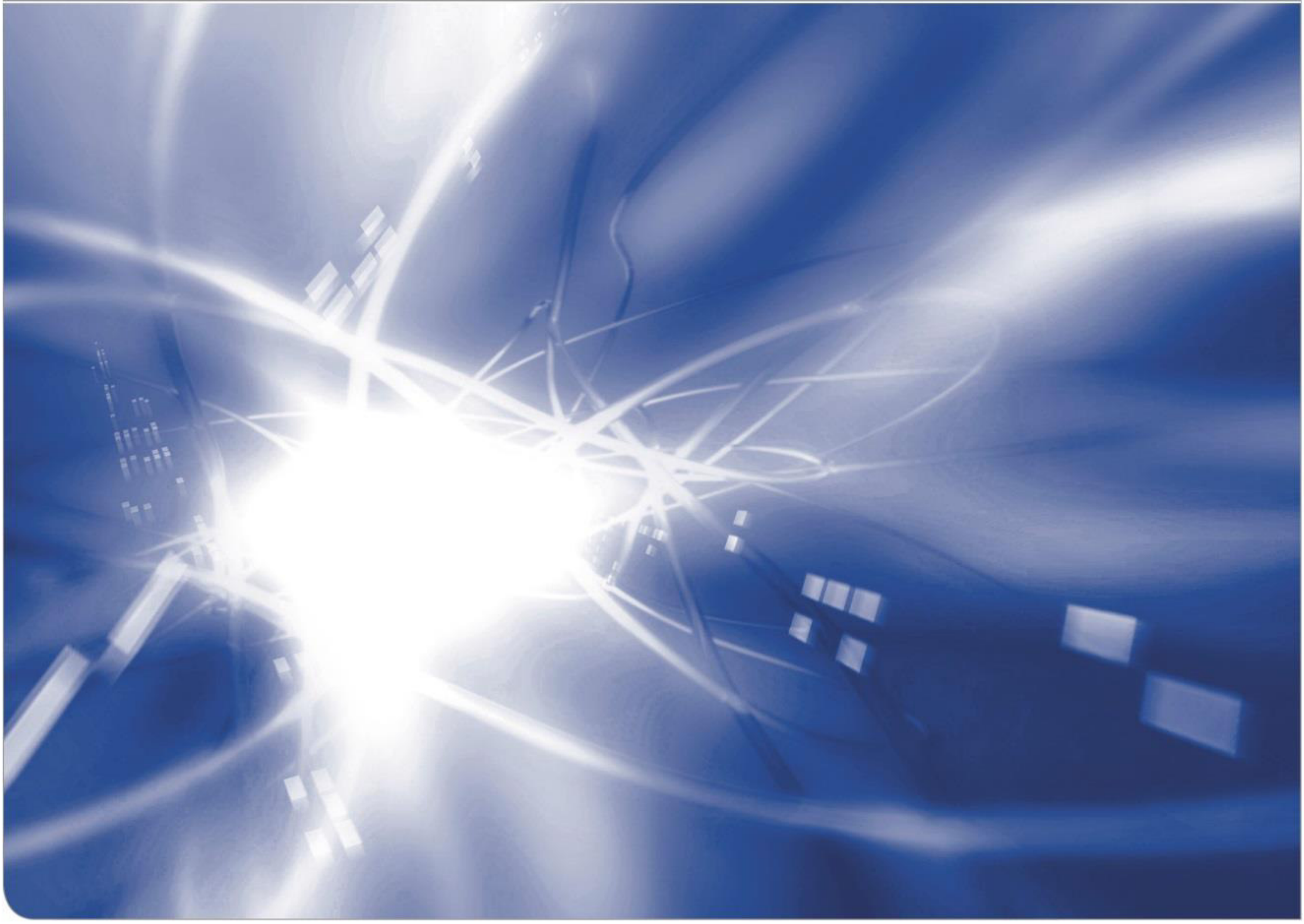

Karlsruhe Institute for Technology
Institute for Applied Materials -
Ceramic Materials and Technologies

Haid-und-Neu Str. 7
D - 76131 Karlsruhe

Impressum

Karlsruher Institut für Technologie (KIT)
www.kit.edu

This document is licensed under the Creative Commons Attribution – Share Alike 4.0 International License (CC BY-SA 4.0): https://creativecommons.org/licenses/by-sa/4.0/deed.en

2017

ISSN: 2194-1629

Abstract

The main advantages of DCDC-specimens, completely stable crack extension and very high path stability due to the strongly negative T-stress term call for an application in R-curve determination. In this report, it is studied whether the T-stress affects the R-curve of silicon nitride.

For this purpose, we selected three Si_3N_4-ceramics, which showed very flat crack resistance curves in test with edge-notched 4-point bending specimens. These materials were tested with DCDC-specimens. In contrast to the bending tests, the crack resistance decreased clearly. This effect can be understood as a consequence of the T-stress term.

Contents

1 What is the T-stress? 1

2 T-stress solutions 2

3 Stability properties of DCDC specimens 3

3.1 Stable crack growth 3

3.2 Path stability 4

4 Example of application: Prediction of bridging effects 5

4.1 Frictional bridges 5

4.2 Debonding 6

5 R-curve measurements via DCDC 8

References 12

1. What is the T-stress?

The stresses in the vicinity of a crack tip are described by a series expansion with respect to the distance *r* from the tip and angular functions $f_{ij}(\varphi)$ as suggested by Williams [1]:

$$\sigma_{ij} = \frac{K_I}{\sqrt{2\pi r}} f_{ij}(\varphi) + \sigma_{ij,0} \ , \tag{1.1}$$

where the coordinate *r* has the origin at the crack tip, Fig. 1.

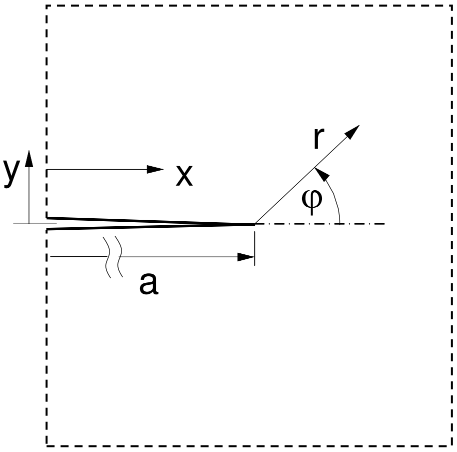

Fig. 1 Geometrical data at a crack tip**.**

The fracture mechanics description of failure at crack tips is mostly focused on the singular stress field governed by the stress intensity factor *K*. This loading parameter is the amplitude of the first series expansion term of (1.1) depending on the crack-tip distance *r* as $1/r^{1/2}$. The first regular stress term in the Williams series expansion [1] is the so-called “T-stress”. The Cartesian components of the first regular term are for traction free crack faces

$$\sigma_{ij,0} = \begin{pmatrix} \sigma_{xx,0} & \sigma_{xy,0} \\ \sigma_{yx,0} & \sigma_{yy,0} \end{pmatrix} = \begin{pmatrix} T & 0 \\ 0 & 0 \end{pmatrix} \tag{1.2}$$

Restricting the description on the singular stress term and the first regular term, the near-tip stress field of a cracked body can be described by

$$\sigma_x = \frac{K_I}{\sqrt{2\pi r}} f_{xx}(\varphi) + T + O(r^{1/2}) \tag{1.3}$$

$$\sigma_y = \frac{K_I}{\sqrt{2\pi r}} f_{yy}(\varphi) + O(r^{1/2}) \tag{1.4}$$

The angular functions are for mode-I loading:

$$f_{xx} = \cos\left(\frac{\varphi}{2}\right)\left[1 - \sin\left(\frac{\varphi}{2}\right)\sin\left(\frac{3\varphi}{2}\right)\right] \tag{1.5}$$

$$f_{yy} = \cos\left(\frac{\varphi}{2}\right)\left[1+\sin\left(\frac{\varphi}{2}\right)\sin\left(\frac{3\varphi}{2}\right)\right] \tag{1.6}$$

On the prospective crack plane it holds simply $f_{xx}(0)=f_{yy}(0)=1$.

Two *important conclusions* may be drawn from eqs.(1.3)-(1.6):

I) Ahead of a crack, $\varphi=0$, the T-stress is negligible compared to the singular stress for $r\rightarrow 0$. Nevertheless, it may be important for effects playing in some distance from the tip as e.g. diffusion effects.

II) In the wake of a crack, $\varphi=\pi$, all singular stresses disappear since $f_{xx}=f_{yy}=0$. This holds because of $\cos(\pi/2)=0$ in eqs.(1.5) and (1.6). With other words: All effects prevailing in the crack wake are affected by the T-stress exclusively.

2. T-stress solutions

In order to allow simple comparison of T-stresses for different test specimens, e.g. 4-point bending with DCDC, it is of advantage to represent the T-stress in a normalized form. Normalization on the stress intensity factor K and the crack length a is possible by use of the biaxiality ratio β according to Leevers and Radon [2]

$$\beta = \frac{T\sqrt{\pi a}}{K_{\mathrm{I}}} \tag{2.1}$$

Results are plotted in Fig. 2a for the DCDC specimen as the symbols. The symbols represent FE results from [3]. For the mostly chosen geometry $H/R=4$, the biaxiality ratio may be expressed for $2\leq a/R\leq 7$ by a simple linear approximation

$$\beta \approx -3\frac{a}{R} \tag{2.2}$$

introduced in Fig. 2a as the straight line.

The biaxiality ratio for a bar is according to [4]

$$\beta = \frac{-0.469+1.2825\alpha+0.6543\alpha^2-1.2415\alpha^3+0.07568\alpha^4}{\sqrt{1-\alpha}}, \quad \alpha=\frac{a}{W}, \tag{2.3}$$

This dependency is shown in Fig. 1b. The square indicates the relative crack depth of $a/W\cong 1/3$ at which the T-stress changes from negative to positive values. R-curve tests in 4-point bending exhibiting starter cracks of $a_0/W\approx 0.5$ always show positive T-stresses, i.e. a crack-parallel tension.

Finally, Fig. 3 gives a comparison for the two test specimens. This figure makes clear that in a DCDC-test the T-stress plays a much stronger role than in a bending test.

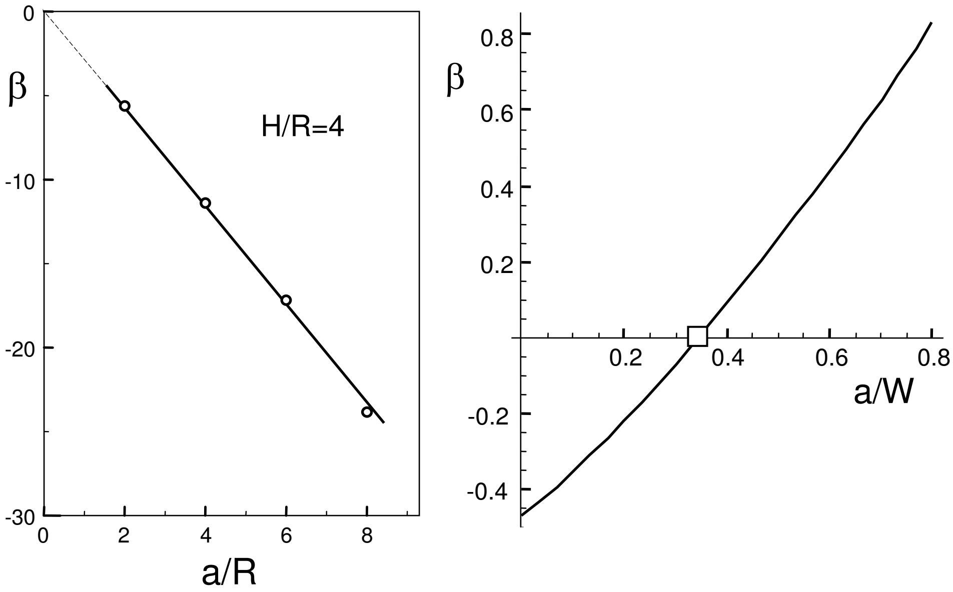

Fig. 2 Biaxiality ratio; a) DCDC: symbols are finite element results [3], line according to eq.(2.2), b) result for the bending bar, by eq.(2.3).

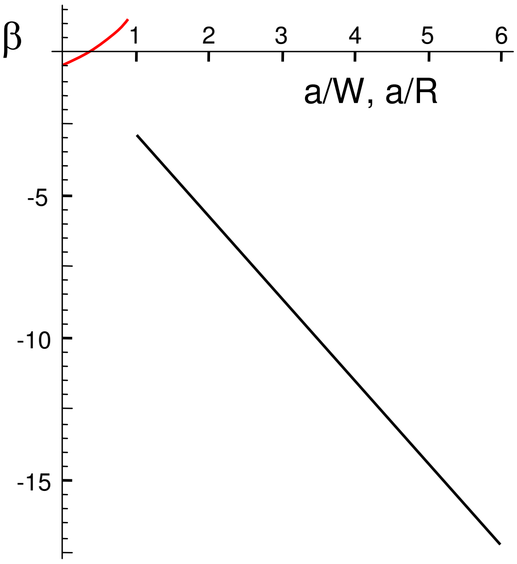

Fig. 3 Comparison of the DCDC-test specimen (black) with the bending bar (red).

3. Stability properties of DCDC specimens

DCDC-tests show excellent benefits in stability. The effect on stable crack propagation (i.e. the absence of accelerated extension and spontaneous fracture) and on plane crack development may be briefly addressed.

3.1 Stable crack growth

The fact that crack extension is stable in a large region of crack lengths is trivial and doesn't need much explanation. A crack extends stably as long as the stress intensity factor decreases with increasing crack length. This is shown in Fig. 4a by the range dK/da<0. At the beginning of crack formation and when the crack approaches the end faces, crack extension is unstable because of dK/da>0.

Crack stability is in other "standard tests" missing as may be shown for the edge-notched bending bar. The stress intensity for a crack in a 4-point-bending test is given in Fig. 4b. Here, the complete region 0<a/W<1 is unstable since dK/da>0 for any crack depth.

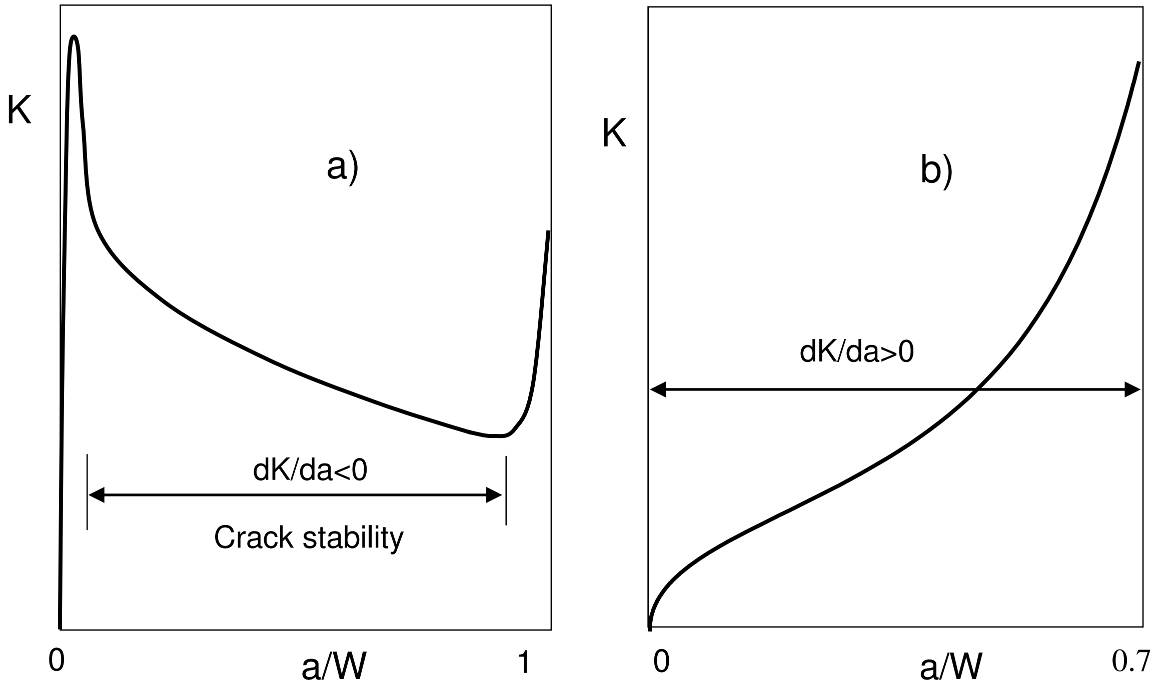

Fig. 4 a) Crack stability in the region of dK/da<0 for the DCDC specimen, b) crack instability for the edge-cracked 4-point bending bar.

3.2 Path stability

A crack of initial length a_0 is considered, which grows out of the initial straight plane by an angle of Θ_0 (Fig. 5). The kink angle Θ_0 may represent the influence of a disturbing mode-II loading caused by a small unavoidable misalignment of the loading arrangement. For small kink angles it holds

$$\Theta_0 = -\frac{2K_{\mathrm{II}}}{K_{\mathrm{I}}} \tag{3.1}$$

where K_{I} and K_{II} are the stress intensity factors for the initial crack situation.

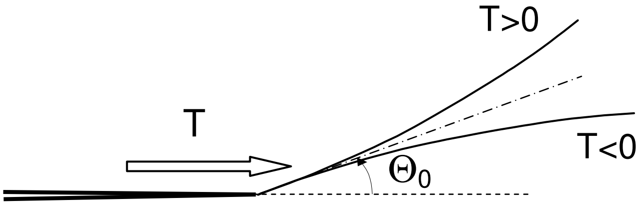

Fig. 5 General influence of the T-stress after crack kinking under mixed-mode loading.

In [5], Cotterell and Rice analysed the local crack path stability where the first deviation from the initial straight crack plane was of interest. At small crack extensions, the deviation from the initial crack plane is illustrated in Fig. 5. For details see Section G2 in [6]).

The most important conclusion of [5] is illustrated in Fig. 5, namely, increasing deviation from the prescribed kink angle for $T>0$ and decreasing deviations for $T<0$.

Cotterell and Rice showed that crack path stability is only guaranteed for $T<0$. In nearly all fracture mechanics test specimens; however, the T-stress terms are positive, at least in the commonly used range of crack lengths.

There are two exceptions for standard test specimens used for ceramics, namely, small cracks in bending bars with a relative crack length $a/W<0.35$ (specimen width W) and the DCDC specimen where the latter shows strongly negative T in the whole range of practically used crack lengths, Fig. 2a.

From the mostly positive sign of the biaxiality ratio for DCDC test specimens and the unavoidable small misalignments, it has to be expected that path stability is guaranteed.

4. Example of application: Prediction of bridging effects

4.1 Frictional bridges

The bridging effects by frictional or elastic crack-face interlocking were described in [4] (see Section B4) and in [6] (Section F1) by application of the bridging model by Mai and Lawn [7].

In the schematic depiction of Fig. 6, a large grain is shown, acting as a frictional crack-bridging event. The x-component of the thermal mismatch tractions σ_{mis} is indicated. For a 3-dimensional analysis, we have to consider crack-face interlocking with a finite depth L in the order of $L \approx D$. The consequence is that mismatch stresses also act in y-direction of Fig. 6 (y-component not plotted in Fig. 6b).

The loads transferred by crack face interactions are localized at single grains. The bridging stress σ_{br} for such an element can be expressed by

$$\sigma_{br} \cong \begin{cases} \mu(\sigma_{mis,x} + \sigma_{mis,y}) & for \quad \sigma_{mis,x} < 0,\ \sigma_{mis,y} < 0 \\ \mu\sigma_{mis,x} & for \quad \sigma_{mis,x} < 0,\ \sigma_{mis,y} > 0 \\ \mu\sigma_{mis,y} & for \quad \sigma_{mis,x} > 0,\ \sigma_{mis,y} < 0 \\ 0 & \qquad else \end{cases} \tag{4.1}$$

Consequently, the near-tip stresses at a bridging event in the crack wake are

$$\sigma_x = \sigma_{mis,x} + T \tag{4.2}$$

$$\sigma_y = \sigma_{mis,y} \tag{4.3}$$

Equation (4.2) makes clear, that the compressive T-stress of the DCDC-specimens must increase the effect of frictional crack face bridging, whereas the tensile T-stress in 4-point bending tests must lower it.

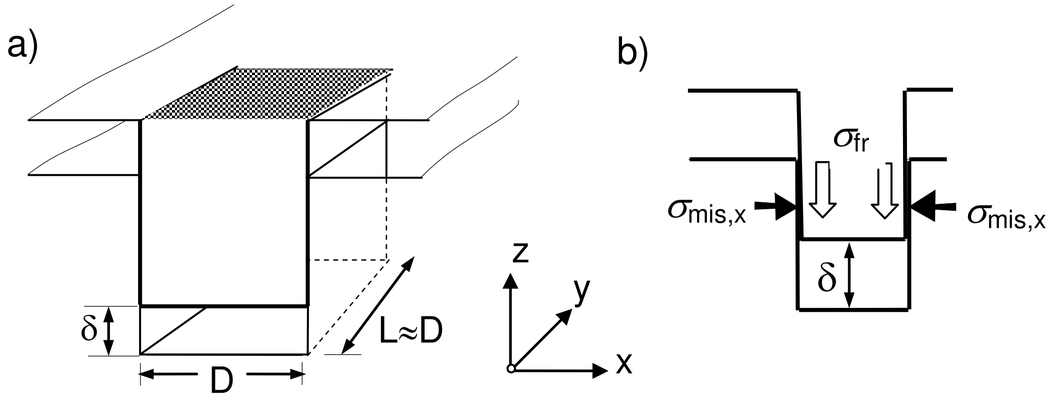

Fig. 6 Crack surface interactions due to a local frictional bridging event, a) geometric data, b) tractions, acting at an interlocking event (tractions in *y*-direction not plotted).

4.2 Debonding

Before a beta-crystal can be pulled out of the matrix and can show frictional bridging, this crystal must first be dissolved from its connection with the matrix. When the crack terminates the crystal-matrix interface, it is stopped, Fig. 7a. There are two possibilities of crack propagation after further load increase. When the strength of the crystal-matrix interface layer is strong enough, the crack-tip stress field will cause fracture of the crystal, Fig. 7b. In case of lower interface strength, the crack will kink and grow along the interface producing a bare neck around the crystal, Fig. 7c. When the crack tip has passed and the singular stresses are missing in the crack wake, the crack opening displacements disappear leaving a closed frictional crystal-matrix contact.

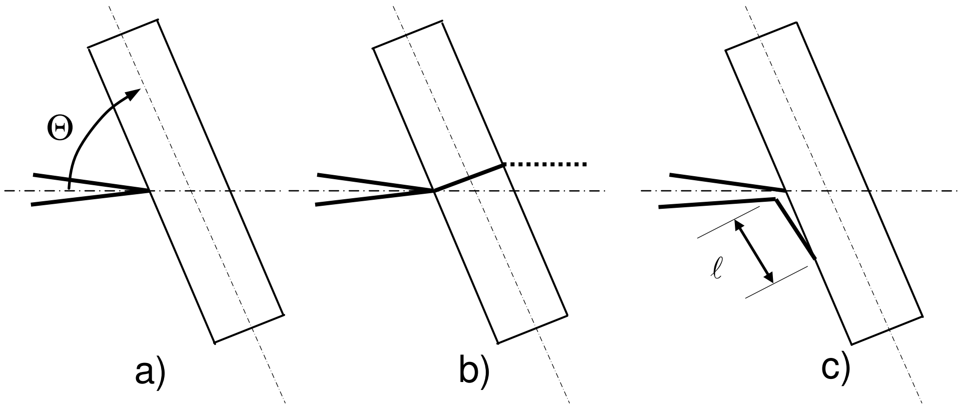

Fig. 7 a) Crack terminating an elongated β-crystal; b) crystal cracking for high grain-boundary strengths, c) crack kinking with following debonding for lower interface strength.

The "strength" of the crystal-matrix interface characterized by the Θ_{cr} at which first dissolving of the interface is observed, has been determined by Becher et al. [8] and Satet and Hoffmann [9,10,11]. For details see also the extended discussion section of

Fünfschilling [12]. The effect of a debond of length ℓ, occurring for an angle smaller of a critical value, $\Theta<\Theta_{cr}$, is shown in Fig. 8 by the black circles. The critical angle is indicated by the black triangle.

Let us now look for the influence of a T-stress. In the approximation of Dundurs-parameters $\alpha=\beta=0$ (e.g. when the E-modulus and the Poisson ratios for a needle-like β-crystal are identical), the stress intensity factors at the tip of the kink can be written as [4]

$$K_{\mathrm{I}}(\ell)=K_{\mathrm{I}}(a)\cos^3(\tfrac{1}{2}\Theta)+T\sqrt{\ell}\sqrt{\tfrac{8}{\pi}}\sin^2\Theta \tag{4.4}$$

$$K_{\mathrm{II}}(\ell)=K_{\mathrm{I}}(a)\cos^2(\tfrac{1}{2}\Theta)\sin(\tfrac{1}{2}\Theta)+T\sqrt{\ell}\sqrt{\tfrac{8}{\pi}}\sin\Theta\cos\Theta \tag{4.5}$$

where $K_{\mathrm{I}}(a)$ is the mode-I stress intensity factor for the straight unkinked crack ($\ell\to 0$). Since T is negative and the absolute value increases with increasing crack length a, the kink stress intensity factors $K_{\mathrm{I}}(\ell)$ and $K_{\mathrm{II}}(\ell)$ and, consequently, the energy release rate $G\propto K_{\mathrm{I}}^2+K_{\mathrm{II}}^2$ decrease too.

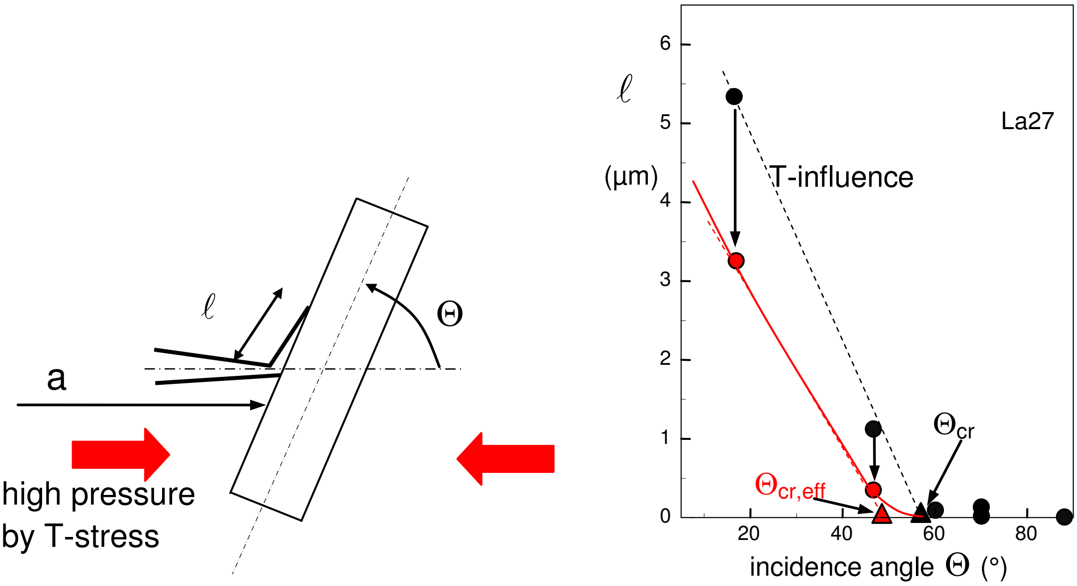

Fig. 8 Influence of T-stress on debonding, a) schematic of debonding, b) comparison with experimental results for an MgLa-doped glass by Satet and Hoffmann [9-11] (black symbols and line), effect of T-stress indicated by the red symbols and line defining an apparent critical incidence angle $\Theta_{\mathrm{cr,eff}}$.

The total energy release rate can be expressed in terms of the effective stress intensity factor K_{eff}

$$K_{eff}=\sqrt{K_{\mathrm{I}}(\ell)^2+K_{II}(\ell)^2} \tag{4.6}$$

Using the biaxiality β ratio proposed by Leevers and Radon [2] as a dimensionless representation of T

$$\beta = \frac{T\sqrt{\pi a}}{K_\mathrm{I}} \tag{4.7}$$

eqs. (4.4-4.6) can be rewritten in

$$\left(\frac{K_{eff}}{K_\mathrm{I}(a)}\right)^2 = \left(\cos^3(\tfrac{1}{2}\Theta) + \beta\sqrt{\frac{8}{\pi}\frac{\ell}{a}}\cos^2\Theta\right)^2 + \left(\cos^2(\tfrac{1}{2}\Theta)\sin(\tfrac{1}{2}\Theta) - \beta\sqrt{\frac{8}{\pi}\frac{\ell}{a}}\cos\Theta\sin\Theta\right)^2 \tag{4.8}$$

For ℓ=0 the critical incidence angle Θ_cr results as

$$\frac{K_{eff}}{K_\mathrm{I}(a)} = \cos^2(\tfrac{1}{2}\Theta_{cr}) \Rightarrow \theta_{cr} = 2\arccos\sqrt{\frac{K_{eff}}{K_I}} \tag{4.9}$$

The kink length ℓ as a function of the incidence angle is given by the zeros of

$$\begin{aligned}\cos^4(\tfrac{1}{2}\Theta_{cr}) = &\left(\cos^3(\tfrac{1}{2}\Theta) + \beta\sqrt{\frac{8}{\pi}\frac{\ell}{a}}\cos^2\Theta\right)^2 + \\ &+\left(\cos^2(\tfrac{1}{2}\Theta)\sin(\tfrac{1}{2}\Theta) - \beta\sqrt{\frac{8}{\pi}\frac{\ell}{a}}\cos\Theta\sin\Theta\right)^2\end{aligned} \tag{4.10}$$

The conclusion from (4.4) and (4.5) on debonding behaviour are illustrated in Fig. 8 together with experimental results by Satet and Hoffmann [9] showing $\Theta_\mathrm{cr}\cong58°$:

1) A kink developing in the case of an angle $\Theta<\Theta_\mathrm{cr}$ remains smaller in a test specimen with strongly negative T-term (DCDC) than in bending. Debonding is suppressed although the Θ may fall clearly below the critical kink angle (Fig. 8). This can be interpreted as a smaller effective critical angle $\Theta_\mathrm{cr,eff}\approx<\Theta_\mathrm{cr}$ defined by the intersection of the linear red curve part. The consequence of the lower critical angle results in a lower number of crystals able to debond considerably. This number is proportional to 1-sin(Θ_cr).
2) With increasing crack length the part of crystals with $\Theta<\Theta_\mathrm{cr}$ able for debonding must show a smaller amount of debonding. The R-curve must decrease with respect to that obtained in a test with $T\approx0$.

Both effects should yield a decrease of the R-curve for a material that shows a flat plateau for specimens with negligible T-stress as for instance the 4-point bending tests.

5. R-curve measurements via DCDC

R-curves for two silicon nitride ceramics were determined in DCDC tests. The materials tested were a hot- isostatically- pressed silicon nitride with 8.5 wt% Lu_2O_3 and 1.93 wt% MgO (denoted as MgLu), a hot- isostatically- pressed silicon nitride with

5 wt% Y_2O_3 and 2 wt% MgO (denoted as MgY) and a commercial silicon nitride with Y_2O_3 and Al_2O_3 content (SL200BG, CeramTec, Plochingen, Germany).

Since the ratio of toughness to Young's modulus, K_R/E, in tests can become clearly larger than in the case of glass, we used shorter specimens (dimension W=6 mm, H=2 mm, R≅0.5 mm, and B=3 mm) in order to avoid any possible buckling effect. During load application the crack length was measured by use of an optical microscope with large focal length. The results are shown in Fig. 9a. The data points are restricted to $a \geq 0.9$ mm for two reasons. First, the stress intensity factor solutions are all limited to $a/R>2$ and should not be extrapolated too much. On the other hand, spontaneous crack initiation results in a minimum initial crack length which was in our case also in the range of several 100 µm. From this point of view, the DCDC-specimen is not appropriate for the determination of the very steep initial R-curves for silicon nitrides. Nevertheless, this specimen gives information on the plateau behaviour of R-curves. From the experiments clearly decreasing R-curves are visible. The same materials tested with pre-notched bending bars showed a distinct plateau as shown in Fig. 9b.

It should be emphasized the results in Fig. 9a and 9b correspond to strongly different crack propagations Δa. A direct comparison is given by Fig. 10.

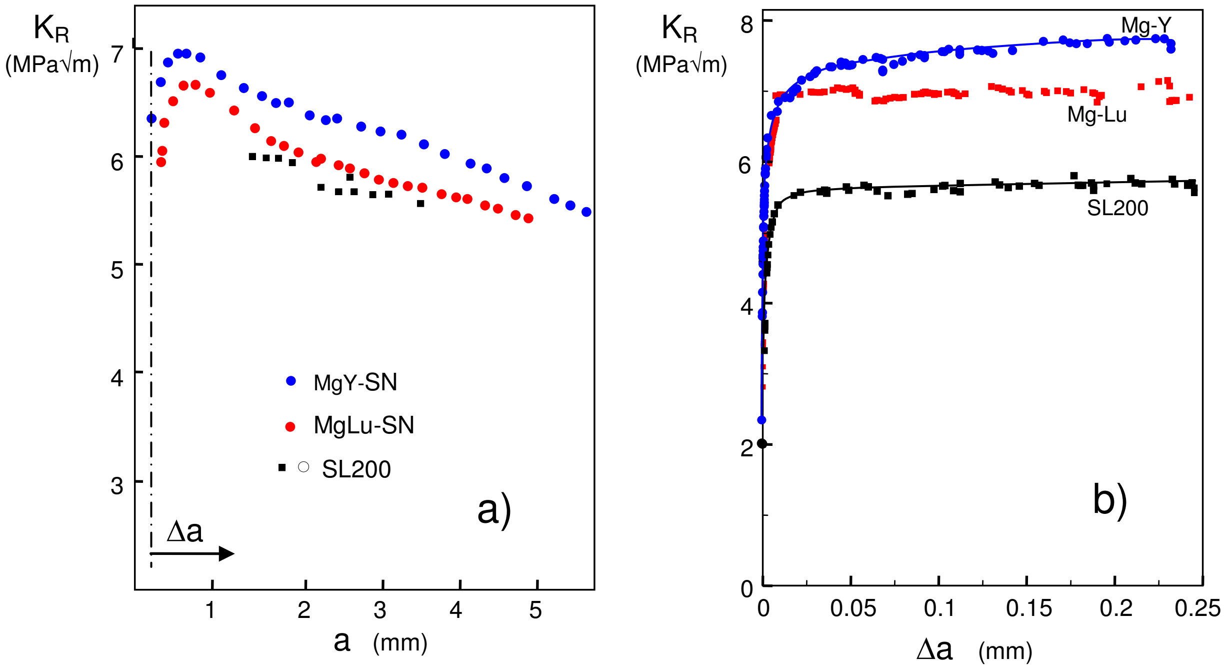

Fig. 9 R-curves for two silicon nitrides containing MgO + Lu_2O_3 and MgO + Y_2O_3 and a commercial material SL200, a) DCDC-specimen, b) edge-notched bending bar.

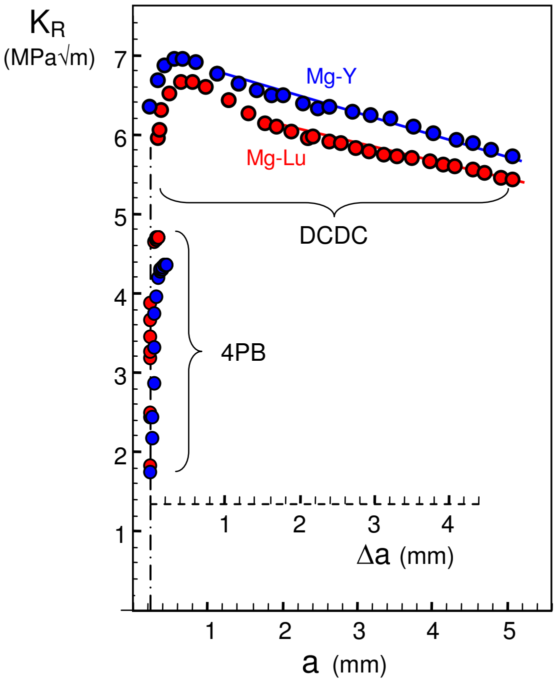

Fig. 10 Direct comparison of the DCDC and edge-notched bending bar tests.

For applications with critical tribological conditions Si_3N_4/SiC-ceramics were fabricated and investigated in DCDC tests. The analysed composite material is gas pressure sintered silicon nitride with 3 wt% Y_2O_3, 3.5 wt% Al_2O_3 as sintering aids and 20 vol% silicon carbide. In this composite material the silicon nitride represents the matrix material and should show comparable behaviour to the commercial silicon nitride SL200BG. In this case lager specimens (dimension W= 40 mm, H= 4 mm, R = 1 mm, and B= 4 mm) were used for the DCDC tests. The results of these tests and of the pre-notched bending bars are shown in Fig. 11.

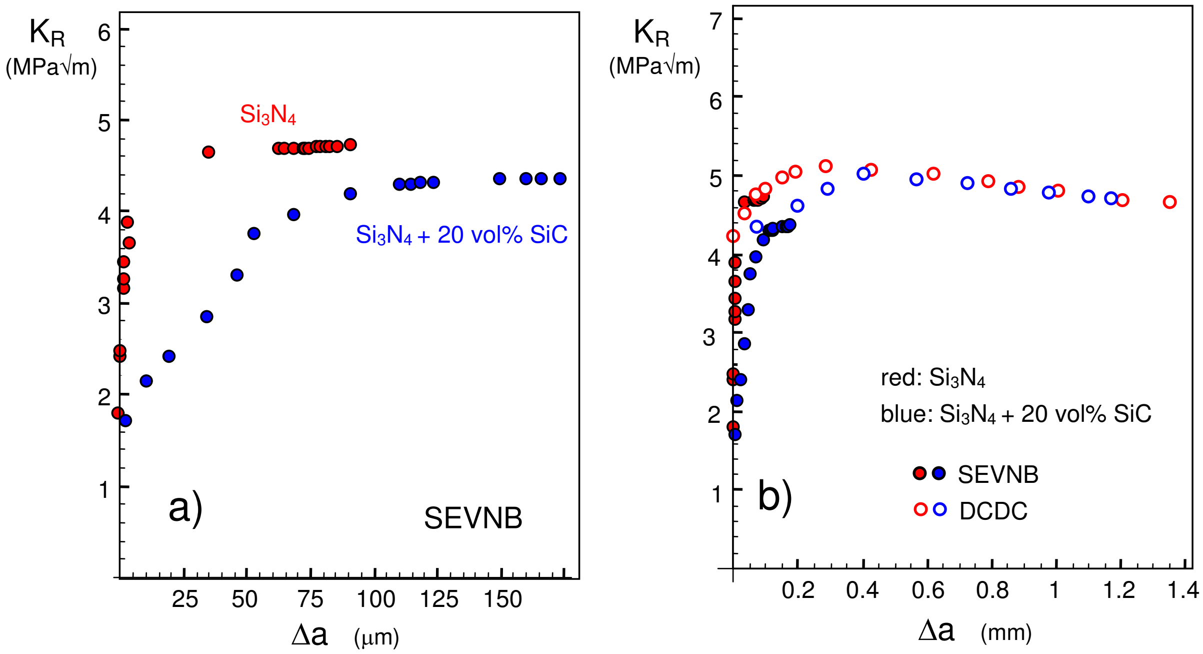

Fig. 11 R-curves for silicon nitrides containing 0 vol% and 20 vol% SiC, a) edge-notched bending bar SEVNB, b) comparison with DCDC results.

The T-stress increases with increasing crack length which results in a decrease in the R-curves at larger crack lengths. Crack-growth resistance K_R versus T-stress are shown in Fig. 12.

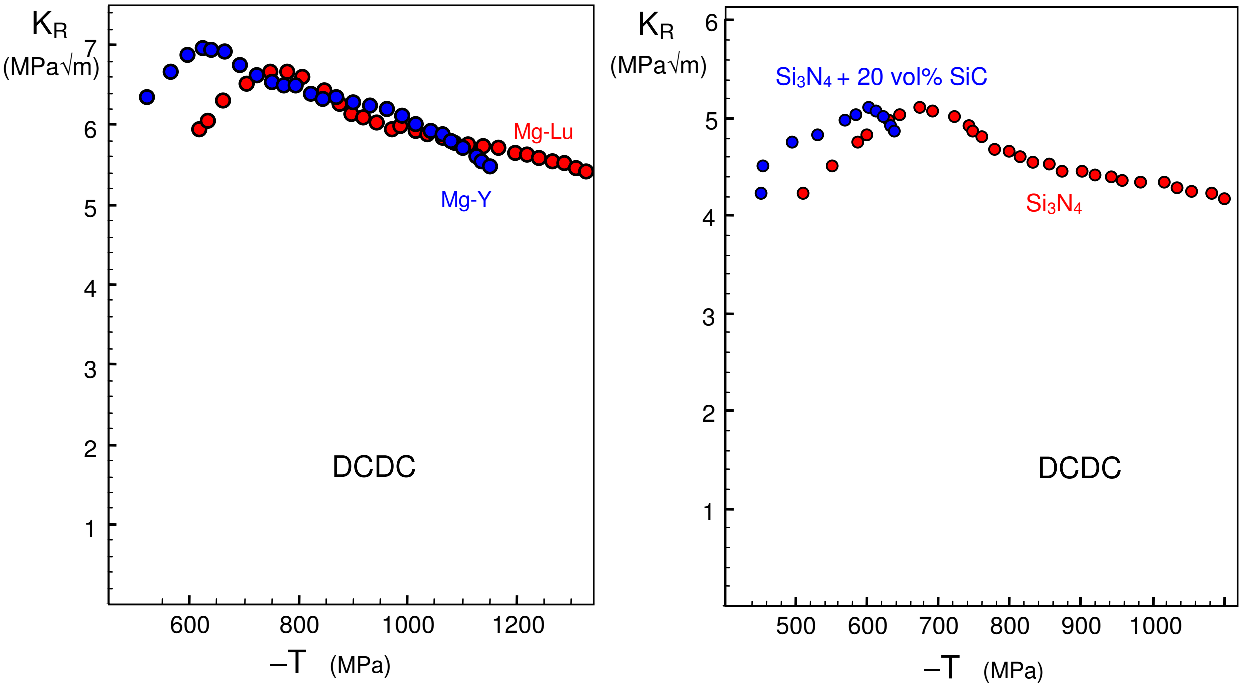

Fig. 12 Crack-growth resistance K_R vs. T-stress.

References

---

[1] Williams, M.L., On the stress distribution at the base of a stationary crack, J. Appl. Mech. **24**(1957), 109-114.

[2] Leevers, P.S., Radon, J.C., Inherent stress biaxiality in various fracture specimen geometries, Int. J. Fract. **19**(1982), 311-325.

[3] Fett, T., Rizzi, G., Guin, J.P., López-Cepero, J.M., Wiederhorn, S.M., A fracture mechanics analysis of the double drilled compression test specimen, Engng. Fract. Mech. **76**(2009), 921-934.

[4] Fett, T., Stress intensity factors, T-stresses, Weight functions, IKM 50, Universitätsverlag Karlsruhe, 2008.

[5] Cotterell, B., Rice, J.R., Slightly curved or kinked cracks, Int. J. Fract., **16**(1980), 155-169.

[6] Fett, T., New contributions to R-curves and bridging stresses – Applications of weight functions, KIT Scientific Publishing, 2012, Karlsruhe.

[7] Mai, Y., Lawn, B.R., Crack-interface grain bridging as a fracture resistance mechanism in ceramics: II. Theoretical fracture mechanics model, J. Am. Ceram. Soc. **70**(1987), 289.

8 Becher, P.F., Sun, E.Y., Hsueh, C.H., Alexander, K.B., Hwang, S.L., Waters, S.B., Westmoreland, C.G.,Debonding of interfaces between beta-Silicon Nitride Whiskers and Si-Al-Y oxinitride glasses, Acta mater., 44(1996), 3881-3893.

9 Satet, R.L., Einfluß der Grenzflächeneigenschaften auf die Gefügeausbildung und das mechanische Verhaltenvon Siliziumnitrid-Keramiken, Dissertation, Universität Karlsruhe, IKM 38, 2002.

10 Satet, R.L., Hoffmann, M.J., Grain growth anisotropy of β-silicon nitride in rare-earth doped oxynitride glasses, J. Eur. Ceram. Soc. **24**(2004), 3437-3445.

11 Satet, R.L., Hoffmann, M.J., Influence of the rare-earth element on the mechanical properties of RE-Mg bearing silicon nitride, J. Am. Ceram. Soc. **88**(2005), 2485-2490.

12 Fünfschilling, S., Mikrostrukturelle Einflüsse auf das R-Kurvenverhalten bei Siliciumnitridkeramiken, Dissertation, KIT-Scientific Publishing, IKM 53, 2010.

KIT Scientific Working Papers
ISSN 2194-1629
www.kit.edu